RESEARCH ARTICLE

A high-resolution view of the coordination environment in a paramagnetic metalloprotein from its magnetic properties

Enrico Ravera[a,b], Lucia Gigli[a,b], Elizaveta A. Suturina[c], Vito Calderone[a,b], Marco Fragai[a,b], Giacomo Parigi[a,b], Claudio Luchinat*[a,b]

This work is dedicated to Ivano Bertini, founder of CERM and pioneer of Biological Inorganic Chemistry, on the 80th anniversary of his birth. The theme of the characterization of metal coordination in biological systems through NMR was a very important part of his research, of which this work is a natural evolution.

[a] Dr. E. Ravera, Ms L. Gigli, Dr. V. Calderone, Prof. M. Fragai, Prof. G. Parigi, and Prof. C. Luchinat
Magnetic Resonance Center (CERM), University of Florence, and Consorzio Interuniversitario Risonanze Magnetiche di Metalloproteine (CIRMMP)
Via L. Sacconi 6, 50019 Sesto Fiorentino, Italy
E-mail: claudioluchinat@cerm.unifi.it
[b] Dr. E. Ravera, Ms L. Gigli, Dr. V. Calderone, Prof. M. Fragai, Prof. G. Parigi, and Prof. C. Luchinat
Department of Chemistry "Ugo Schiff"
University of Florence
Via della Lastruccia 3, 50019, Sesto Fiorentino, Italy
[c] Dr. E. A. Suturina
Department of Chemistry
University of Bath
Claverton Down, Bath BA2 7AY, United Kingdom

Supporting information for this article is given via a link at the end of the document.

Abstract: Metalloproteins constitute a significant fraction of the proteome of all organisms and their characterization is critical for both basic sciences and biomedical applications. A large portion of metalloproteins bind paramagnetic metal ions, and paramagnetic NMR has been widely used in their structural characterization. However, the signals of nuclei in the immediate vicinity of the metal center are often broadened beyond detection. In this work, we show that it is possible to determine the coordination environment of the paramagnetic metal in the protein at a resolution inaccessible to other techniques. Taking the structure of a diamagnetic analogue as a starting point, a geometry optimization is carried out by fitting the pseudocontact shifts obtained from first principles Quantum Chemical calculations to the experimental ones.

Introduction

The metal coordination in metalloenzymes is a key determinant of their function. Understanding the finest details of the metal coordination environment at the highest possible resolution is required to improve the reliability of structure-activity relationships and, in particular, is crucial to the successful use of docking strategies for drug discovery.[1–8]

A molecular property that reflects the very fine details of the metal coordination environment is the magnetic susceptibility χ, a symmetric, rank-two tensor. The magnetic susceptibility is determined in any characterization of magnetic materials, where it can be measured through SQUID or torque magnetometry, or polarized neutron scattering.[9–12] It is less common to realize that the magnetic susceptibility of a metal center also makes its mark on the NMR spectra of the molecule that bears the paramagnetic center: the resonances of each NMR-active nucleus in the molecule experience shifts, called pseudocontact shifts (PCS), that depend on the position of the nucleus with respect to the reference frame defined by the metal center and the principal axes of its magnetic susceptibility tensor. PCS are adequately described by the Kurland-McGarvey equation:[13,14]

$$\delta_{PCS} = \frac{1}{12\pi r^3} Tr\left[\Delta\boldsymbol{\chi} \cdot \left(\frac{3\boldsymbol{r}\boldsymbol{r}^T}{r^2} - \mathbf{1}\right)\right] \quad (1)$$

where $\boldsymbol{r}$ is the vector connecting the nucleus and the paramagnetic center and $\Delta\boldsymbol{\chi} = \boldsymbol{\chi} - 1/3\, Tr(\boldsymbol{\chi}) \cdot \mathbf{1}$. This relationship has been recently validated by a rigorous Quantum Chemical (QC) treatment.[15] In a metalloprotein, PCS remain accurately measurable up to several tens of ångströms from the metal, therefore hundreds of PCS can be reliably measured.[16] Owing to their spatial dependence, PCS have been extensively used for structural determination studies of biological systems.[17–27]

Since PCS ultimately depend on the $\Delta\boldsymbol{\chi}$ tensor, they are being increasingly employed to evaluate magnetic properties and underlying ligand field parameters in the context of molecular magnetism.[28–32] In a paramagnetic metalloprotein, a large number of signals can be observed, and thus provide a very accurate and robust measure of the anisotropy of the magnetic susceptibility.[33]

The improved computational efficiency and quality of relativistic wavefunction-based QC methods[34] allow for the fast and reliable calculation of the magnetic susceptibility of metal complexes from first principles.[35–37] There is now a number of examples where relativistic CASSCF calculations, with second-order perturbation theory corrections, successfully predict the magnetic properties of metal complexes and their temperature dependencies from the molecular structure.[36–38] It is therefore possible to relate the experimental observations to the QC prediction of the magnetic susceptibility magnitude and orientation obtained from the structure of the metal coordination sphere.[10,36,39–41] Magnetic

susceptibility as a structural reporter is sensitive to structural details at a resolution that is one-two orders of magnitude better than the best resolution achieved so far by X-ray or Cryo-EM (Fig. 1).[37,42,43]

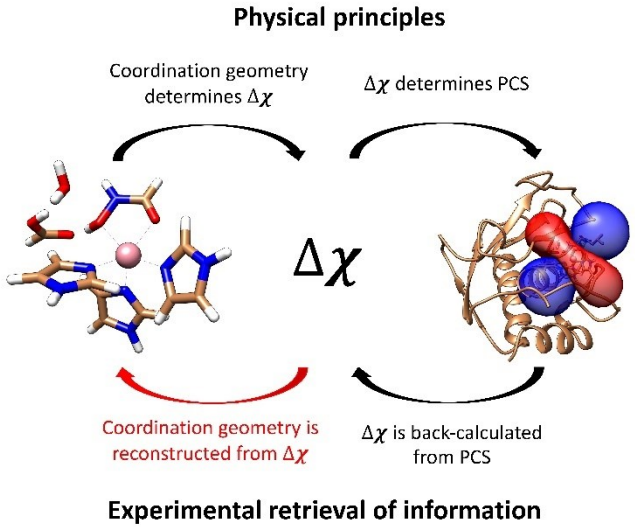

Figure 1. Physical principles correlate the coordination geometry to the PCS through $\Delta\chi$ (top). While $\Delta\chi$ is easily back-calculated from PCS, reconstruction of the coordination geometry from $\Delta\chi$ (bottom left) is novel and is at the core of this work.

Building on these grounds, we propose an approach to determine the coordination environment of a cobalt(II) metalloprotein from PCS measurements. We apply this approach to characterize the metal binding site of the catalytic domain of human matrix metalloproteinase 12 (CoMMP-12), a 17 kDa metalloprotein, coordinated by the inhibitor N-isobutyl-N-[4-methoxyphenylsulphonyl]glycyl hydroxamic acid (NNGH), and in which the native zinc(II) metal center is replaced with high-spin cobalt(II).[44] Cobalt substitution has long been known as a powerful tool for zinc bioinorganic chemistry, because it does not only yield similar coordination geometry but also similar reactivity.[45–47] In the present case, the cobalt(II) enzyme is active, and inhibited by NNGH as is the zinc(II) enzyme.[48,49] The X-ray structure of the NNGH-inhibited zinc(II) enzyme is used as the starting point for the high resolution determination of the coordination environment in the NNGH-inhibited cobalt(II) enzyme in solution. In this effort, we have found that a minor structural perturbation of the starting structure is needed to obtain a very good fit of the experimental PCS and, unexpectedly, we have found that an additional proton needs to be considered in the active site for the experimental data to be satisfied.

Results and Discussion

The ^{13}C PCS measured for CoMMP-12 (taken from reference [50]) can be reproduced very well (Fig. S1) by fitting[51] the $\Delta\chi$ tensor to the carbon coordinates in the X-ray structure of ZnMMP-12 (PDB entry 5LAB[52]). This is not surprising since the bulk of the protein structure is bound to be the same for both metal derivatives. Once the experimental $\Delta\chi$ tensor is available, it can be used to optimize the geometry of the first coordination sphere by minimizing the difference between QC-calculated and experimental PCS values.

All the *ab initio* calculations were carried out using the ORCA 4.2.0 quantum chemistry computational package.[53,54] The magnetic susceptibility tensors were computed using state-averaged complete active space self-consistent field (SA-CASSCF),[55,56] accounting for the dynamic correlations by N-electron valence perturbation theory to the second order (NEVPT2).[57,58] The segmented all-electron relativistically contracted version of Ahlrichs' polarized basis sets[59,60] and the second-order Douglas−Kroll−Hess Hamiltonian (DKH)[61] were employed to account for the scalar relativistic effects. The active space was chosen to contain seven electrons in five cobalt 3*d*-based molecular orbitals. The spin−orbit coupling (SOC) was treated using the mean field (SOMF)[62] approximation as implemented in ORCA. The parameters for the calculations are given in Table 1.

Table 1. Details of the calculations.

	Geometry optimization	Final magnetic properties calculation
Method	~~SOC~~-CASSCF(7,5)	~~SOC~~-CASSCF(7,5)/NEVPT2
Quartets	10	10
Doublets	11	40
Basis set for Co	DKH-def2-TZVP	DKH-def2-TZVP
Basis set for other atoms	DKH-def2-SVP	DKH-def2-TZVP

To mitigate the computational cost, the geometry refinement requires a selection of the atoms to be included in the calculations, and of the degrees of freedom to be adjusted among coordination bond lengths, angles and dihedral angles, without altering the structure of the ligands themselves. The 19 degrees of freedom selected for geometry optimization are shown in Table S1 and S2 and Fig. S2. The selected degrees of freedom are adjusted through a steepest descent search,[63–65] minimizing the disagreement between calculated and experimental PCS. The implemented numerical procedure is represented in Scheme 1.

Definitions

Disagreement function $f = \frac{\sum_i^N(\delta_{calc}^i - \delta_{exp}^i)^2}{\sum_i^N(\delta_{exp}^i)^2}$

Gradient $\mathbf{G}_{f,i} = \left(\frac{f(\mathbf{v}_i-(h_1,0,\ldots,0))-f(\mathbf{v}_i)}{h_1},\ldots,\frac{f(\mathbf{v}_i-(0,0,\ldots,h_n))-f(\mathbf{v}_i)}{h_n}\right)$

Degrees of freedom vector at the *i-th* step $\mathbf{v}_i$: see column 2 Table S2

Increments vector $\mathbf{h}$: see column 6 Table S1

Step scaling factor a = 0.25, 0.5,…, 3.5

Procedure

0) CASSCF/NEVPT2 calculation of the χ tensor for the initial model.

1) Calculation of $\mathbf{G}_{f,i}$:
   a) independent variation of the selected degrees of freedom (Table S2);
   b) CASSCF calculation of the χ tensor for the generated models;
   c) calculation of f and $\mathbf{G}_{f,i}$;

2) Determination of α_{opt}:
   a) generation of 14 models by changing the coordinates according to $\mathbf{G}_{f,i}$: $\mathbf{v}_{temp} = \mathbf{v}_i - \alpha_{temp}\mathbf{G}_{f,i}$;
   b) CASSCF/NEVPT2 calculation of the χ tensor for the generated models;
   c) calculation of f.
   Selection of α_{opt} as the one providing the steepest descent of f.

3) Update of the degrees of freedom: $\mathbf{v}_{i+1} = \mathbf{v}_i - \alpha_{opt}\mathbf{G}_{f,i}$.

The procedure is repeated until f is reduced to within the experimental uncertainty.

Scheme 1. Numerical steepest descent geometry optimization. See Supporting Information for further details.

Starting from the 5LAB structure (Fig. 2), we obtained the initial reduced models composed of: the metal, the three imidazole rings of H218, H222, and H228, the carboxylate of E219, one water molecule,[52] and either the hydroxamate (model A, Fig. 2) or the hydroxamic acid (model B, Fig. 2) moiety of the NNGH inhibitor.

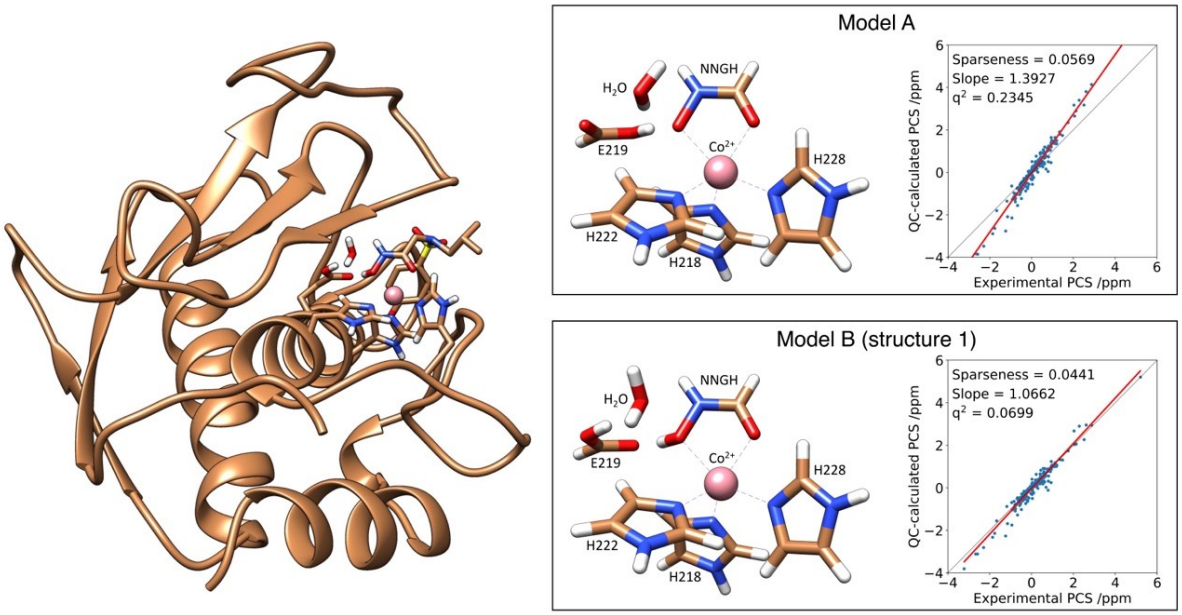

Figure 2. Left: CoMMP-12 protein structure with details of the active site. Right: models of the active site used for the calculations with the hydroxamate (model A) or the hydroxamic acid (model B, structure 1) moieties of the NNGH inhibitor, and the corresponding agreements between QC-calculated and experimental PCS.

The different protonation state of the NNGH results in sizable differences in the *ab initio* calculated magnetic susceptibility anisotropy: in the situation depicted in model A, the optimization of the hydrogen positions invariably shifts the proton from NNGH to E219, confirming the picture adopted by most MMP researchers.[66–69] However, the anisotropy of the susceptibility obtained from this model is too large with respect to the experimental one (as highlighted by the too large slope of the regression line of Model A, Fig. 2). Conversely, if the hydroxamate is protonated, the anisotropy of the susceptibility decreases sizably, getting much closer to the experimental value (as highlighted by the slope almost equal to 1 of the regression line of Model B, Fig. 2). To force protonation of the hydroxamate ligand, a second proton bound to E219 is needed (model B). This proton distribution in the active site may have interesting implications for the mode of action of MMPs, as it will be discussed later.

In four steps of geometry refinement of model B, the agreement between the QC-calculated and the experimental data becomes very good (Tables S3-S6 and Fig. S3).

To prove the robustness of the results, we have performed additional calculations where either the basis set or the size of the reduced model were modified. In particular:

1) the PCS calculated with the basis set used for the intermediate steps of the PCS-driven geometry optimization and with more complete basis sets is equally good (Fig. S43), and a perfect correlation between PCS calculated with different basis sets is obtained (Fig. S54);

2) the comparison of the PCS calculated with the DKH-def2-SVP basis set for all atoms with the experimental ones confirms that a) the addition of a proton in the active site is needed (cfr. model A and model B, structure 1, Fig. S65) and that b) the optimization yields a better agreement with the experimental data (cfr. model B, structures 1 and 4, Fig. S65);

3) including the hydrogen bonding partners of all the metal ligands in the model used for the calculation of the magnetic properties does not alter significantly the quality of the fit for the final structure (Model B, structure 4, Fig. S76).

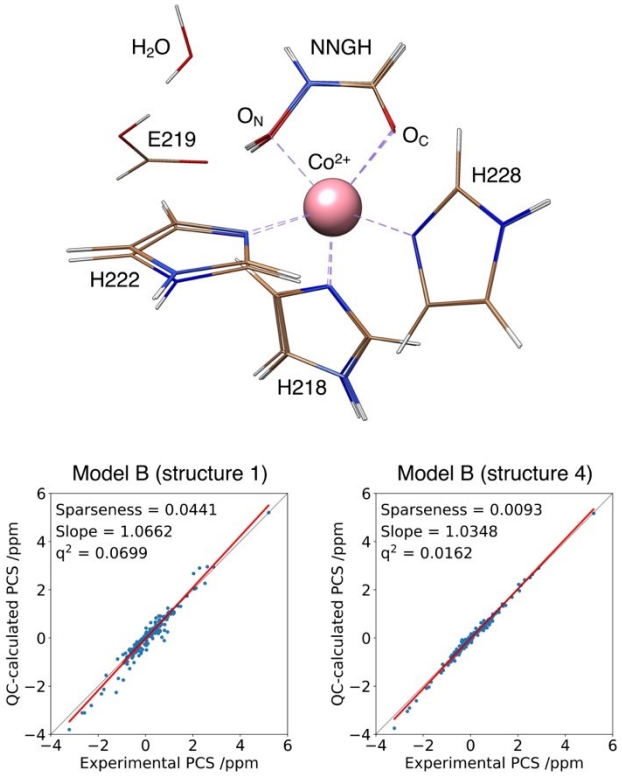

Figure 3. Top: comparison of structures 1 and 4, respectively before and after geometry refinement of model B. Bottom: agreement between experimental and QC-calculated PCS for both structures.

Finally, even changing completely the approach to the calculation of the magnetic susceptibility does not seem to play a crucial role. We have calculated the magnetic susceptibility from the Spin Hamiltonian (SH) parameters using the semiempirical formulation of the Van Vleck equation instead of directly as the second derivative of the energy with respect to the magnetic field, as implemented in ORCA. Of note, the *ab initio* determination of SH parameters at the CASSCF-NEVPT2 is amply benchmarked.[70–73] Although the semiempirical approach is more approximate, the results are in remarkable agreement with those of the direct calculation of the magnetic susceptibility, and confirm all the structural conclusions drawn in this work (Fig. S87).

In principle, an ambiguity in the structural results could arise from the fact that different geometrical modifications of the CoMMP-12 coordination sphere could yield the same magnetic susceptibility tensor, and therefore the same agreement to the experimental PCS. However, the steepest descent minimization ensures that the movement is towards the local minimum that is geometrically the closest to the starting coordinates. Indeed, the first coordination sphere structure of CoMMP-12 obtained from the PCS-driven optimization still fits into the ZnMMP-12 electron density map (Fig. 4, Supporting Information, Table S7 and Figs. S98-S109 for details).

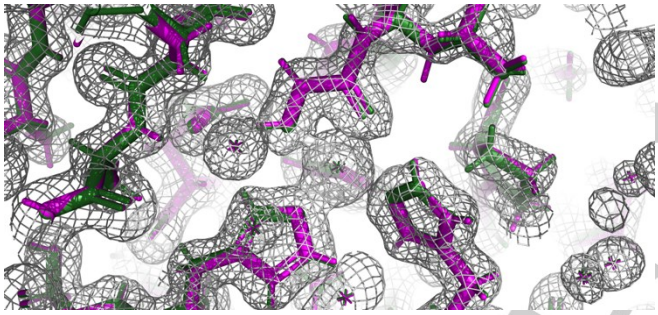

Figure 4. $2F_O$-F_C map of ZnMMP-12 with the original structure in yellow and the constrained one in green. The density is shown at 1.0σ.

It is important to underline that the geometry optimization presented here does not constitute a refinement of the low-temperature X-ray structure of the zinc(II) derivative. Here, we obtain a stand-alone refined structure in solution at room temperature of the active site of the cobalt(II) enzyme, having only used the zinc(II) enzyme structure as the starting model.
The general applicability of this method will increase with the continuously increasing computational power, which will soon allow us to find the absolute minimum even by starting from a more distant initial structure, or from structures of lower quality, or even from homology models.
The initial and final structures are so similar as to be hardly distinguishable (Fig. 3, Table S2). However, it is possible to notice that:
1) the hydroxamic acid fragment gets closer to the metal;
2) H222 tends to decrease the angle formed with the metal and the NNGH O_C, and
3) H218 tends to decrease the angle formed with the metal and H228.
These structural differences, which are relatively modest (Table S6), can be rationalized by comparing the position of the ligands with respect to the axes of the experimental and QC-calculated magnetic susceptibility tensors (Fig. 5 and Fig. S110).
All these structural features witness a level of "resolution" in the active site that can be estimated at the picometer scale and therefore well beyond that presently attainable by any structural method in solution.

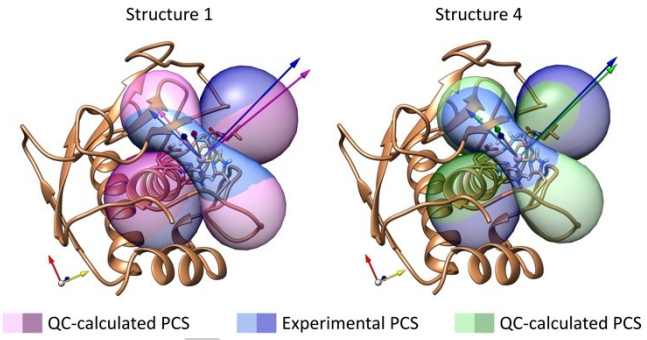

Figure 5. Comparison of the isoPCS surfaces (calculated at ±1.5 ppm) of experimental and QC-calculated PCS for structures 1 and 4.

Of note, the magnetic anisotropy in structure 4 is smaller than in structure 1 (Table 2) due to a larger ligand field associated with the shorter Co-N218 distance (2.044 Å compared to 2.075 Å) that defines the main axis of the ligand field (Fig. S124, panel a) of a distorted square pyramidal coordination (Fig. S132). The energy of the first excited state that largely determines the magnetic anisotropy is connected with the splitting between the d_{xy} and d_{xz} orbitals; the d_{xz} orbital is destabilised due to π-antibonding interaction with the H218 π-system and this effect becomes more pronounced as the Co-N218 bond shortens (Fig. S124, panel b).

Table 2. Comparison of the experimental magnetic susceptibility anisotropy tensor with *ab initio* calculated (CASSCF(7,5)/NEVPT2) tensors at 298 K for structures 1 and 4 (see Table S8 for the full $\Delta\chi$ tensors).

	$\Delta\chi_{ax}$	$\Delta\chi_{rh}$	α	β	γ
	10^{-32} m^3	10^{-32} m^3	°	°	°
Str.1	10.4	-4.95	-102.42	-77.97	-105.08
Str.4	9.71	-4.67	-70.33	-98.93	-70.58
Exp.	10 ± 0.1	-2.8 ± 0.1	-75±1	-98.2±0.5	68.6±0.2

Coordination chemists are inclined to think that metal coordination geometries impose rather stiff restraints to the molecular shape. However, it has long been known that metalloproteins are not canonical coordination systems, because the protein itself poses significant strains to the idealised geometries and, in some cases, this is related to function.[74] Even for the present low-symmetry system, we find it instructive to relate the starting and the minimized structures to ideal geometries. In ranging from octahedral to tetrahedral coordination, high-spin cobalt(II) can pass through different flavours of pentacoordination (see chapter 7 of reference [16]). In the present case, the structure of the first coordination sphere is intermediate between square pyramidal and trigonal bipyramidal (see Table S9 and Fig. S132, S143), and the refinement brings it somewhat closer to the latter.

The protonation state of the hydroxamate ligand in inhibited MMPs has been a subject of debate in the early years of the discovery of this class of enzymes, which are of potential pharmacological interest due to their implication in inflammation and in the spreading of metastatic cells (see [67], [75], and references therein). Carboxylic acids have pKas around 5, while hydroxamic acids have pKas around 9, so at a physiological pH of around 7 it would be expected that E219 is deprotonated and anionic, and the hydroxamic inhibitor protonated and neutral. However, multiple experimental evidences point to a situation where the proton forms an H-bond between the two groups and is actually residing mostly on E219, leaving a negative hydroxamate moiety. This has been rationalized by considering that the bulky hydroxamic inhibitor completely occludes the active site cavity, so that the carboxylate moiety of E219 is not accessible to solvent molecules. Under these conditions a low dielectric environment is created, and the pKa of E219 can increase by several units, while the negative charge of the hydroxamate can be stabilised by the dipositive zinc (or in our case cobalt) cation. As described above, attempts to predict by computations the position of the proton shared between these two groups invariably point to a negative hydroxamate group and a protonated, neutral E219 (model A, Fig. 6), in agreement with the expectations. However, a neutral hydroxamic moiety and a still neutral E219 (model B, Fig. 6) yield a magnetic susceptibility anisotropy much closer to the experimental one. This computationally suggested arrangement of protons in the active site of MMPs could provide a plausible explanation for the proton uptake observed by calorimetry when hydroxamic acid inhibitors bind the enzyme: E219 could be deprotonated in the free enzyme but could regain a proton from the hydroxamic acid moiety, which in turn could regain a proton from the solvent. In the free, active enzyme, protonation of E219 by a metal coordinated water molecule, which then becomes a hydroxide ion, has also been invoked to explain the efficient nucleophilic attack on the peptide bond, which constitutes the first step of the hydrolytic action of the enzyme.[75,76]

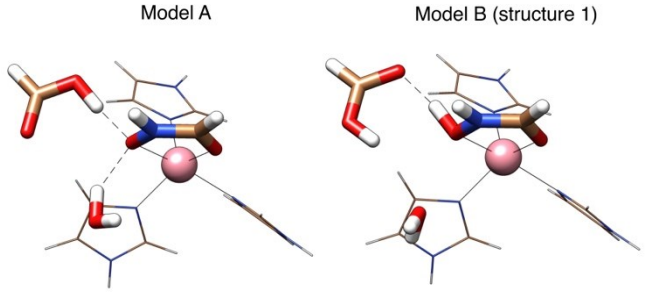

Figure 6. Comparison of model A and model B (structure 1) with the hydrogen bonds represented as dashed lines. For clarity, NNGH, E219, and the water molecule are shown as sticks, while the imidazole rings are traced as wires.

The presence of metal centers is challenging for all structural techniques: X-ray diffraction (XRD) may suffer from density flattening in the vicinity of the metal,[77] for cryo-EM the reconstruction may be complicated by the density deviations of metals from the average electron distribution of proteins.[78] EXAFS can, in principle, provide metal coordination geometries with interatomic distances and angles that are significantly more accurate than those provided by XRD or Cryo-EM. However, EXAFS is limited to the immediate vicinity of the metal ion and is poorly sensitive to protons.

NMR signals observed in the immediate vicinity of the metal center are subject to Fermi-contact shifts (FCS), which are proportional to the electron spin densities on the observed nuclei.[16] FCS of metal ligands can be as large as several hundreds of ppm and may be reporters of the coordination geometry at the metal center.[79–82] Recently, a QC approach has been employed to select one among a few structural models of the cobalt(II) coordination sphere in the active site of human superoxide dismutase 1, on the basis of the FCS from 7 nearby nuclei.[83]

Nuclei in the immediate vicinity of the metal center can also be observed in EPR-based approaches (ENDOR, ESEEM, HYSCORE).[84–89] These approaches are also particularly powerful in (e.g.) detecting protonation states,[90,91] but these measurements usually require low to very low temperatures (below 10 K for high-spin cobalt(II)), which may alter the local structure at the metal center. As for FCS in NMR, also in EPR-based approaches, only a limited number of hyperfine couplings can be obtained. In the present case, the situation is further complicated by the presence of as many as 13(14) protons in the first coordination sphere of the metal, making it problematic to assess the correct protonation state (Tables S10, S11).

The approach we present here relies, instead, on many shifts - measured in solution at room temperature - that can be used to determine with high accuracy the magnetic susceptibility anisotropy. The latter is currently calculated from first principles with higher accuracy than electron spin densities, which means that PCS are calculated more accurately than FCS.[70,92–95]

Concluding remarks

We describe a method to determine with very high accuracy the coordination sphere of a paramagnetic metal ion in a metalloprotein that combines experimental determination and quantum chemical calculations of NMR observables. We have applied this method to the determination of the active site structure of the enzymatically active CoMMP-12.

The results of this work demonstrate that the *ab initio* quantum chemical calculations of paramagnetic NMR observables have improved so much that their combination with experiments can now reveal the structural features of the coordination environment of metalloenzyme active sites. We expect that, with the increase in computational power, more complex systems will become accessible in this way, providing a further tool in the hands of bioinorganic chemists.

Acknowledgements

This work has been supported by the Fondazione Cassa di Risparmio di Firenze, and the Italian Ministero dell'Istruzione, dell'Università e della Ricerca through the "Progetto Dipartimenti di Eccellenza 2018-2022" to the Department of Chemistry "Ugo Schiff" of the University of Florence, and the University of Florence through the "Progetti Competitivi per Ricercatori" to ER. LG acknowledges the support of an EMBO Short-Term Fellowship (ASF8629). We acknowledge the CINECA award to ER under the ISCRA initiative, for the availability of high-performance computing resources and support. The authors acknowledge the support and the use of resources of Instruct-

ERIC, a landmark ESFRI project, and specifically the CERM/CIRMMP Italy center.

Keywords: Metal coordination • *Ab initio* magnetic susceptibility • Magneto-structural correlations

[1] I. V. Korendovych, W. F. DeGrado, Current Opinion in Structural Biology 2014, 27, 113–121.
[2] S. Signorella, C. Palopoli, G. Ledesma, Coordination Chemistry Reviews 2018, 365, 75–102.
[3] V. Kairys, M. K. Gilson, M. X. Fernandes, The Scientific World JOURNAL 2006, 6, 1542–1554.
[4] C. Oshiro, E. K. Bradley, J. Eksterowicz, E. Evensen, M. L. Lamb, J. K. Lanctot, S. Putta, R. Stanton, P. D. J. Grootenhuis, J. Med. Chem. 2004, 47, 764–767.
[5] S. L. McGovern, B. K. Shoichet, J. Med. Chem. 2003, 46, 2895–2907.
[6] A. Bordogna, A. Pandini, L. Bonati, J. Comput. Chem. 2011, 32, 81–98.
[7] D. J. Diller, R. Li, J. Med. Chem. 2003, 46, 4638–4647.
[8] P. Ferrara, E. Jacoby, J Mol Model 2007, 13, 897–905.
[9] K. Ridier, B. Gillon, A. Gukasov, G. Chaboussant, A. Cousson, D. Luneau, A. Borta, J.-F. Jacquot, R. Checa, Y. Chiba, H. Sakiyama, M. Mikuriya, Chem. Eur. J. 2016, 22, 724–735.
[10] G. Cucinotta, M. Perfetti, J. Luzon, M. Etienne, P.-E. Car, A. Caneschi, G. Calvez, K. Bernot, R. Sessoli, Angewandte Chemie International Edition 2012, 51, 1606–1610.
[11] M. Perfetti, E. Lucaccini, L. Sorace, J. P. Costes, R. Sessoli, Inorg. Chem. 2015, 54, 3090–3092.
[12] M. Perfetti, Coordination Chemistry Reviews 2017, 348, 171–186.
[13] H. M. McConnell, The Journal of Chemical Physics 1957, 27, 226–229.
[14] R. J. Kurland, B. R. McGarvey, J.Magn.Reson. 1970, 2, 286–301.
[15] L. Lang, E. Ravera, G. Parigi, C. Luchinat, F. Neese, J. Phys. Chem. Lett. 2020, acs.jpclett.0c02462.
[16] I. Bertini, C. Luchinat, G. Parigi, E. Ravera, NMR of Paramagnetic Molecules: Applications to Metallobiomolecules and Models, Elsevier, Amsterdam, 2017.
[17] M. Gochin, H. Roder, Bulletin of Magnetic Resonance 1995, 17, 1–4.
[18] L. Banci, I. Bertini, K. L. Bren, M. A. Cremonini, H. B. Gray, C. Luchinat, P. Turano, J.Biol.Inorg.Chem. 1996, 1, 117–126.
[19] I. Bertini, A. Donaire, B. Jimènez, C. Luchinat, G. Parigi, M. Piccioli, L. Poggi, J.Biomol.NMR 2001, 21, 85–98.
[20] I. Bertini, P. Kursula, C. Luchinat, G. Parigi, J. Vahokoski, M. Willmans, J. Yuan, Journal of the American Chemical Society 2009, 131, 5134–5144.
[21] L. Banci, I. Bertini, G. Cavallaro, A. Giachetti, C. Luchinat, G. Parigi, J.Biomol.NMR 2004, 28, 249–261.
[22] S. Balayssac, I. Bertini, C. Luchinat, G. Parigi, M. Piccioli, Journal of the American Chemical Society 2006, 128, 15042–15043.
[23] D. Sala, A. Giachetti, C. Luchinat, A. Rosato, J Biomol NMR 2016, 66, 175–185.
[24] C. Schmitz, A. M. J. J. Bonvin, J Biomol NMR 2011, 50, 263–266.
[25] C. A. Salgueiro, D. L. Turner, A. V. Xavier, Eur J Biochem 1997, 244, 721–734.
[26] K. Yamamoto, U. H. N. Dürr, J. Xu, S.-C. Im, L. Waskell, A. Ramamoorthy, Sci Rep 2013, 3, 2538.
[27] H. Lee, T. Polenova, R. H. Beer, A. E. McDermott, J. Am. Chem. Soc. 1999, 121, 6884–6894.
[28] M. Hiller, T. Sittel, H. Wadepohl, M. Enders, Chem. Eur. J. 2019, 25, 10668–10677.
[29] M. Hiller, S. Krieg, N. Ishikawa, M. Enders, Inorg. Chem. 2017, 56, 15285–15294.
[30] T. Morita, M. Damjanović, K. Katoh, Y. Kitagawa, N. Yasuda, Y. Lan, W. Wernsdorfer, B. K. Breedlove, M. Enders, M. Yamashita, J. Am. Chem. Soc. 2018, 140, 2995–3007.
[31] V. V. Novikov, A. A. Pavlov, Y. V. Nelyubina, M.-E. Boulon, O. A. Varzatskii, Y. Z. Voloshin, R. E. P. Winpenny, J. Am. Chem. Soc. 2015, 137, 9792–9795.
[32] V. V. Novikov, A. A. Pavlov, A. S. Belov, A. V. Vologzhanina, A. Savitsky, Y. Z. Voloshin, J. Phys. Chem. Lett. 2014, 5, 3799–3803.
[33] G. Parigi, E. Ravera, C. Luchinat, Progress in Nuclear Magnetic Resonance Spectroscopy 2019, 114–115, 211–236.
[34] T. Helgaker, S. Coriani, P. Jørgensen, K. Kristensen, J. Olsen, K. Ruud, Chem. Rev. 2012, 112, 543–631.
[35] L. F. Chibotaru, L. Ungur, The Journal of Chemical Physics 2012, 137, 064112.
[36] E. A. Suturina, J. Nehrkorn, J. M. Zadrozny, J. Liu, M. Atanasov, T. Weyhermüller, D. Maganas, S. Hill, A. Schnegg, E. Bill, J. R. Long, F. Neese, Inorg. Chem. 2017, 56, 3102–3118.
[37] M. Atanasov, D. Aravena, E. Suturina, E. Bill, D. Maganas, F. Neese, Coordination Chemistry Reviews 2015, 289–290, 177–214.
[38] P. Kumar, D. J. SantaLucia, K. Kaniewska-Laskowska, S. V. Lindeman, A. Ozarowski, J. Krzystek, M. Ozerov, J. Telser, J. F. Berry, A. T. Fiedler, Inorg. Chem. 2020, 59, 16178–16193.
[39] L. Rigamonti, N. Bridonneau, G. Poneti, L. Tesi, L. Sorace, D. Pinkowicz, J. Jover, E. Ruiz, R. Sessoli, A. Cornia, Chem. Eur. J. 2018, 24, 8857–8868.
[40] M. Vonci, K. Mason, E. A. Suturina, A. T. Frawley, S. G. Worswick, I. Kuprov, D. Parker, E. J. L. McInnes, N. F. Chilton, J. Am. Chem. Soc. 2017, 139, 14166–14172.
[41] A. A. Pavlov, J. Nehrkorn, Y. A. Pankratova, M. Ozerov, E. A. Mikhalyova, A. V. Polezhaev, Y. V. Nelyubina, V. V. Novikov, Phys. Chem. Chem. Phys. 2019, 21, 8201–8204.
[42] M. Briganti, G. F. Garcia, J. Jung, R. Sessoli, B. Le Guennic, F. Totti, Chem. Sci. 2019, 10, 7233–7245.
[43] D. Parker, E. A. Suturina, I. Kuprov, N. F. Chilton, Acc. Chem. Res. 2020, 53, 1520–1534.
[44] S. Balayssac, I. Bertini, A. Bhaumik, M. Lelli, C. Luchinat, Proc.Natl.Acad.Sci.USA 2008, 105, 17284–17289.
[45] I. Bertini, C. Luchinat, Acc.Chem.Res. 1983, 16, 272–279.
[46] I. Bertini, C. Luchinat, Adv.Inorg.Biochem. 1985, 6, 71–111.
[47] A. Donaire, J. Salgado, H. R. Jimenez, J. M. Moratal, in Nuclear Magnetic Resonance of Paramagnetic Macromolecules, Springer Dordrecht, 1995.
[48] I. Bertini, M. Fragai, Y.-M. Lee, C. Luchinat, B. Terni, Angew.Chem.Int.Ed. 2004, 43, 2254–2256.
[49] S. P. Salowe, A. I. Marcy, G. C. Cuca, C. K. Smith, I. E. Kopka, W. K. Hagmann, J. D. Hermes, Biochemistry 1992, 31, 4535–4540.
[50] S. Balayssac, I. Bertini, M. Lelli, C. Luchinat, M. Maletta, K. J. Yeo, Journal of the American Chemical Society 2007, 129, 2218–2219.
[51] M. Rinaldelli, A. Carlon, E. Ravera, G. Parigi, C. Luchinat, Journal of Biomolecular NMR 2015, 61, 21–34.
[52] L. Benda, J. Mareš, E. Ravera, G. Parigi, C. Luchinat, M. Kaupp, J. Vaara, Angew. Chem. Int. Ed. 2016, 55, 14713–14717.
[53] F. Neese, WIREs Comput Mol Sci 2012, 2, 73–78.
[54] F. Neese, WIREs Comput Mol Sci 2018, 8, DOI 10.1002/wcms.1327.
[55] B. O. Roos, P. R. Taylor, P. E. M. Sigbahn, Chemical Physics 1980, 48, 157–173.
[56] P. E. M. Siegbahn, J. Almlöf, A. Heiberg, B. O. Roos, The Journal of Chemical Physics 1981, 74, 2384–2396.
[57] C. Angeli, R. Cimiraglia, Theoretical Chemistry Accounts: Theory, Computation, and Modeling (Theoretica Chimica Acta) 2002, 107, 313–317.
[58] C. Angeli, R. Cimiraglia, S. Evangelisti, T. Leininger, J.-P.

Malrieu, The Journal of Chemical Physics 2001, 114, 10252–10264.
[59] A. Schäfer, C. Huber, R. Ahlrichs, The Journal of Chemical Physics 1994, 100, 5829–5835.
[60] F. Weigend, R. Ahlrichs, Phys. Chem. Chem. Phys. 2005, 7, 3297.
[61] B. A. Hess, Phys. Rev. A 1986, 33, 3742–3748.
[62] D. Ganyushin, F. Neese, The Journal of Chemical Physics 2013, 138, 104113.
[63] A. Lunghi, S. Sanvito, arXiv:1903.01424 [cond-mat, physics:quant-ph] 2019.
[64] A. Lunghi, F. Totti, S. Sanvito, R. Sessoli, Chem. Sci. 2017, 8, 6051–6059.
[65] A. Lunghi, F. Totti, R. Sessoli, S. Sanvito, Nat Commun 2017, 8, 14620.
[66] V. Borsi, V. Calderone, M. Fragai, C. Luchinat, N. Sarti, Journal Medicine Chemistry 2010, 53, 4285–4289.
[67] J. Cha, D. S. Auld, Biochemistry 1997, 36, 16019–16024.
[68] C. M. Holman, C. C. Kan, M. R. Gehring, H. E. Van Wart, Biochemistry 1999, 38, 677–681.
[69] M. H. Parker, E. A. Lunney, D. F. Ortwine, A. G. Pavlovsky, C. Humblet, C. G. Brouillette, Biochemistry 1999, 38, 13592–13601.
[70] S. K. Singh, M. Atanasov, F. Neese, J. Chem. Theory Comput. 2018, 14, 4662–4677.
[71] E. A. Suturina, D. Maganas, E. Bill, M. Atanasov, F. Neese, Inorg. Chem. 2015, 54, 9948–9961.
[72] I. Nemec, R. Herchel, I. Svoboda, R. Boča, Z. Trávníček, Dalton Trans. 2015, 44, 9551–9560.
[73] M. Idešicová, J. Titiš, J. Krzystek, R. Boča, Inorg. Chem. 2013, 52, 9409–9417.
[74] B. L. Vallee, R. J. Williams, Proceedings of the National Academy of Sciences 1968, 59, 498–505.
[75] I. Bertini, V. Calderone, M. Fragai, C. Luchinat, M. Maletta, Angew.Chem.Int.Ed. 2006, 45, 7952–7955.
[76] J. A. Jacobsen, J. L. Major Jourden, M. T. Miller, S. M. Cohen, Biochimica et Biophysica Acta (BBA) - Molecular Cell Research 2010, 1803, 72–94.
[77] B. D. Belviso, R. Caliandro, D. Siliqi, V. Calderone, F. Arnesano, G. Natile, Chem. Commun. 2013, 49, 5492.
[78] M. Spiegel, A. K. Duraisamy, G. F. Schröder, Journal of Structural Biology 2015, 191, 207–213.
[79] I. Bertini, C. Luchinat, G. Parigi, R. Pierattelli, Dalton Trans. 2008, 3782.
[80] I. Bertini, C. Luchinat, G. Parigi, F. A. Walker, J.Biol.Inorg.Chem. 1999, 4, 515–519.
[81] M. D. Liptak, X. Wen, K. L. Bren, Journal of the American Chemical Society 2010, 132, 9753–9763.
[82] T. E. Machonkin, W. M. Westler, J. L. Markley, Inorganic Chemistry 2005, 44, 779–797.
[83] A. Bertarello, L. Benda, K. Sanders, A. J. Pell, M. J. Knight, V. Pelmenschikov, L. Gonnelli, I. C. Felli, M. Kaupp, L. Emsley, R. Pierattelli, G. Pintacuda, J. Am. Chem. Soc. 2020, jacs.0c07339.
[84] M. Kampa, W. Lubitz, M. van Gastel, F. Neese, J Biol Inorg Chem 2012, 17, 1269–1281.
[85] M. Stein, W. Lubitz, Journal of Inorganic Biochemistry 2004, 98, 862–877.
[86] I. L. McConnell, V. M. Grigoryants, C. P. Scholes, W. K. Myers, P.-Y. Chen, J. W. Whittaker, G. W. Brudvig, J. Am. Chem. Soc. 2012, 134, 1504–1512.
[87] S. Van Doorslaer, B. Cuypers, Molecular Physics 2018, 116, 287–309.
[88] W. Lubitz, H. Ogata, O. Rüdiger, E. Reijerse, Chem. Rev. 2014, 114, 4081–4148.
[89] A. Silakov, E. J. Reijerse, W. Lubitz, Eur. J. Inorg. Chem. 2011, 2011, 1056–1066.
[90] M. Kampa, M.-E. Pandelia, W. Lubitz, M. van Gastel, F. Neese, J. Am. Chem. Soc. 2013, 135, 3915–3925.
[91] W. K. Myers, E. N. Duesler, D. L. Tierney, Inorg. Chem. 2008, 47, 6701–6710.
[92] F. Neese, The Journal of Chemical Physics 2001, 115, 11080–11096.
[93] F. Neese, The Journal of Chemical Physics 2003, 118, 3939–3948.
[94] F. Neese, J. Phys. Chem. A 2001, 105, 4290–4299.
[95] E. Ravera, L. Gigli, B. Czarniecki, L. Lang, R. Kümmerle, G. Parigi, M. Piccioli, F. Neese, C. Luchinat, Inorg. Chem. 2021, acs.inorgchem.0c03635.

Entry for the Table of Contents

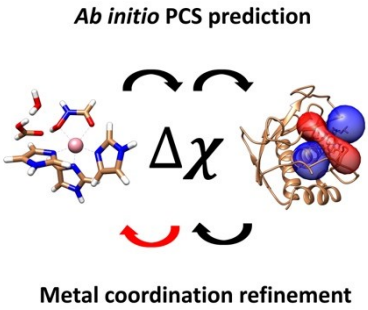

A close look from a distance: pseudocontact shifts depend on the magnetic susceptibility of the metal center, which in turn depends on the coordination geometry. We exploit these dependencies to obtain a detail view of metal coordination in a metalloprotein.

Institute and/or researcher Twitter usernames: @CERM_CIRMMP